Malaysian Journal of Chemistry, 2024, Vol. 26(5), 72-89
(Special Issue: *3rd Virtual International Symposium on Sciences 2023*)

Exploring SB2OME and Metal Complexes as Antibacterial Agents: Synthesis, Characterization and Molecular Docking

Siti Khadijah Roslan[1], Fiona N. -F How[1]*, Zalikha Ibrahim[2,3] and Nurasyikin Hamzah[1]
[1]Department of Chemistry, Kulliyyah of Science,
[2]Department of Pharmaceutical Chemistry, Kulliyyah of Pharmacy
[3]Drug Discovery and Synthesis Research Group, Kulliyyah of Pharmacy
International Islamic University Malaysia (IIUM), 25200, Kuantan, Pahang, Malaysia
*Corresponding author (e-mail: howfiona@gmail.com)

A series of new substituted dithiocarbazate, *S*-benzyl-β-*N*-2-methoxybenzoyl dithiocarbazate (SB2OME), and its metal complexes have been successfully synthesised and characterised. SB2OME was synthesised *via* condensation of *S*-benzyldithiocarbazate (SBDTC) with 2-methoxybenzoyl chloride before complexing with various metal ions to yield a tridentate ONS Cu(II), Zn(II), Co(II), and Ni(II) complexes. All compounds underwent characterization *via* various physico-chemical analyses. Antibacterial activities of all the compounds were evaluated against *Staphylococcus aureus* (ATCC 25923) and *Escherichia coli* (ATCC 25922). ADMET prediction was utilised to assess drug-likeness. The molecular docking was used against mutant and wild-type DNA gyrase *B* receptor *E. coli* (PDB:1AJ6 and 4WUB) to evaluate whether the bioactivities of the compounds are in correlation with the mechanism of DNA supercoiling. *In-vitro* analysis demonstrated that SB2OME and its metal complexes exhibit certain effectiveness against *S. aureus* and *E. coli*, and their potency, as measured by MIC values, is significantly inferior to that of well-established antibiotics. The ADMET prediction showed that SB2OME and its metal complexes possess favourable drug-likeness properties. From the molecular docking study, all the synthesised compounds prefer to bind with wild-type compared to the mutant DNA gyrase *B*. However, the absence of agreement between the binding energy and experimental results indicates that DNA gyrase B might not be the possible mechanism of action for the investigated compounds, as compared to their MIC values. Hence, this study concluded the necessity for structural modifications to enhance potency and effectiveness against pathogenic bacteria, alongside exploring additional computational methods to gain a deeper understanding of how newly synthesized compounds exert their mechanism of action.

Keywords: Dithiocarbazate derivatives; metal complexes; antimicrobial; ADMET; molecular docking

Received: October 2023; Accepted: February 2024

The rising global death toll from bacterial infections and the emergence of multi-drug resistant strains due to antibiotic overuse represent a severe threat to humanity today [1]. Antimicrobial resistance (AMR) is anticipated to overtake all other global causes of death in the following decades. According to estimates by Murray et al. (2020), 1.3 million of the expected 4.95 million deaths in 2019 are directly attributable to AMR [2]. Therefore, new lead compounds are urgently required to facilitate the development of next-generation antibiotics. Metal complexes have played a minor yet crucial as antibacterial agents. Unfortunately, the development of penicillin and subsequent antibiotics has reduced the clinical usage of metal-based antibacterial agents [3]. There are currently more metal-based anticancer agents compared to antibacterial agents. One contributing factor would be that metal is considered a systemic toxicant that can cause metal toxicity. However, it is crucial to recognize that the human body requires a small concentration of metal ions to facilitate the enzyme function in the body, oxygen transport, and maintain proper pH balance. Some examples of essential metals include zinc, iron, copper, magnesium, and calcium. These metals have a vital role as cofactors or active components in various enzyme reactions necessary for biological processes [4]. When combined with a biologically active ligand, a metal ion can operate as a transporter, allowing it to enter a particular cell location and exhibit its antibacterial action [5]. This is because physiologically active ligands are substances regularly taken up by bacterial cells. Compared to non-metal-based antibiotics, the incorporation of metal ions may adapt novel mechanisms of action [6]. Additionally, metal ions can pharmacologically stabilise several bioactive compounds, navigating their administration to the target [7]. Dithiocarbazate derivatives have recently garnered significant due to their promising bioactivity against various bacterial cells [8-9]. Owing to the presence of nitrogen and sulfur donor atoms in the structure of dithiocarbazate, they are feasible to bind with metal ions to give metal complexes, enhancing

†Paper presented at the 3rd Virtual International Symposium on Sciences (3rd VISoS 2023)

the therapeutic properties of the compound [10]. Antibacterial research has shown that metal complexes from dithiocarbazate derivatives are typically more effective than their parent ligands against the investigated bacterial strains [11-12]. Thus, metal-based medicines from dithiocarbazate derivative are required as potential antibacterial agents in response to the substantial rise in AMR.

Conventional "trial and error" approaches to discovering effective antibacterial leads are costly and time-consuming [13]. Furthermore, significant problems persist, especially in the absorption, distribution, metabolism, elimination, and toxicity (ADMET) processes during drug development. Consequently, ADMET analysis of the compounds becomes crucial during the development process. To ascertain whether a compound is orally active, Lipinski's rule of five (RO5) can be used to evaluate the drug-likeness of the compound. According to RO5, an orally active drug candidate must fulfil four out of the five requirements, which are: (a) having fewer than ten hydrogen bond acceptor groups; (b) having fewer than five hydrogen bond donor groups; (c) having a molecular weight below 500; (d) having an octanol-water partition coefficient (log P) below five; and (e) having a topological polar surface area (TPSA) below 140 $Å^2$ [14]. Applying these criteria not only streamlines the drug development process but increases the likelihood of identifying a compound with greater efficiency. Apart from good ADMET properties, a promising drug candidate must also have good binding interaction with a targeted protein. Such interaction can be observed *via* experimental methods such as X-ray crystallography or computational methods such as molecular docking. Generally, molecular docking is a computational method widely employed in drug design and discovery due to its affordability, usefulness, and effectiveness [15]. The algorithm within the molecular docking software has been developed based on experimental data to predict not only the binding interaction but also the binding affinity between a drug molecule and biological target, as well as their preferred conformation and orientation. The molecular docking can be conducted at the pre-screening or post-screening step, depending on the purpose of the research. Due to this versatility, molecular docking has been proven to be valuable in the process of designing more active ligands [16].

Considering the growing need for safe and effective bioactive compounds to combat bacteria infections, this study aimed to discover the *in-vitro* and *in-silico* properties of SB2OME and its Cu(II), Zn(II), Co(II), and Ni(II) metal complexes. The characterisation of the compounds encompasses a range of analytical and spectroscopy techniques, including melting point analysis, FT-IR spectroscopy, UV-Vis spectroscopy, NMR spectroscopy, magnetic susceptibility, and molar conductivity measurements. The compounds underwent screening for antibacterial activity against Gram-positive and Gram-negative bacteria, specifically *Staphylococcus aureus* (ATCC 25923) and *Escherichia coli* (ATCC 25922), respectively. Additionally, the ADMET analysis was performed using SwissADME and Protox-II to assess the drug-likeness and toxicity of these compounds. Subsequently, a molecular docking study was conducted to investigate possible mechanisms of action of compounds at the mutant (R136H) and wild type 4WUB of DNA gyrase subunit B (GyrB) from *E. coli* using AutoDock 4.2.

EXPERIMENTAL

Chemicals

The solvent and chemicals used in this study were 2-methoxylbenzoyl chloride, benzyl chloride, hydrazine hydrate, carbon disulfide, copper(II) acetate monohydrate, nickel(II) acetate tetrahydrate, zinc(II) acetate dihydrate, cobalt(II) acetate tetrahydrate, potassium hydroxide, absolute ethanol, silica gel, dimethyl sulfoxide, potassium bromide, nutrient agar, nutrient broth, gentamycin. All solvents and chemicals were used as received without purification and were purchased from Hmbg® Chemicals, Acros Organics, Merck, Sigma Aldrich, R&M Chemicals, Bendosen, Fisher Scientific, Himedia, and VWR Life Science.

Instruments

Melting points were determined using Electrothermal™ IA9300. The IR spectra were recorded in the range of 400-4000 cm^{-1} with KBr pellets on a FTIR Perkin Elmer (FTIR Frontier). The molar conductance of a 10^{-3} M solution of each metal complex in DMSO was measured at 26 ºC using an Eutech CON 700 conductivity meter. The UV–VIS spectra were recorded on a Shimadzu UV-1900 Series PC spectrophotometer (800–200 nm) in DMSO solution. ^1H NMR and ^{13}C NMR spectra were recorded in DMSO-d_6 on the NMR Bruker Ultra Shield Plus 500 MHz spectrometer. Magnetic susceptibility was measured with a Sherwood Scientific MSB AUTO at 298 K.

Synthesis Method

Synthesis of S-benzyl Dithiocarbazate (SBDTC)

The synthesis of SBDTC was performed with some modified procedures following Ali et al. (1977) [17]. Potassium hydroxide (0.1 mol, 5.7 g) was dissolved in 35 ml cold 90% ethanol, and hydrazine hydrate (0.1 mol, 5 ml) was subsequently added to this solution. The mixture was cooled in an ice bath until the temperature reached 0 °C. To the resultant cooled solution, carbon disulphide (0.1 mol, 6 ml) was added dropwise over an hour with constant stirring using a mechanical stirrer to obtain two layers. The brown oil (lower layer) was obtained and dissolved in 30 ml cold 40% ethanol. The solution was kept in an ice bath

(0-5 °C), and benzyl chloride (0.1 mol, 11.37 ml) was added dropwise with vigorous stirring. Precipitate was obtained after the addition of benzyl chloride addition, filtered, and dried overnight over blue indicating silica gel. Lastly, it was recrystallised from hot ethanol to obtain the pure product.

Synthesis of S-benzyl-β-N-2-methoxybenzoyl Dithiocarbazate (SB2OME)

SB2OME was prepared according to the method reported by How et al. (2008) [18]. SBDTC (0.01 mol, 1.983 g) was dissolved in 30 ml absolute ethanol mixed with potassium hydroxide (0.01 mol, 0.56 g) in 10 ml ethanol. 2-methoxybenzoyl chloride (0.01 mol, 1.42 ml) was added dropwise to the solution with constant stirring and heating. After the complete addition of 2-methoxybenzoyl chloride, the resulting solution was allowed to heat and stir to reduce the volume to half. The white product was filtered while hot and dried over blue, indicating silica gel overnight. Lastly, it was recrystallised from hot ethanol to get the pure product.

General Synthesis of Metal Complexes

The same general method was used to prepare the metal complexes $Cu(SB2OME)_2$, $Zn(SB2OME)_2$, $Co(SB2OME)_2$, and $Ni(SB2OME)_2$. The metal complexes were prepared following a previous report [18]. SB2OME (0.9 mmol, 0.3 g) was dissolved in boiling ethanol (30 ml), which was added to a hot solution of metal salt (0.45 mmol) that dissolved in boiling ethanol (30 ml) was added to a hot solution of metal salt (0.45 mmol) dissolved in the same solvent (30 ml). The mixture was heated and stirred until the volume was reduced to half at approximately 20 minutes. The precipitate was filtered while hot and dried over blue, indicating silica gel overnight. The metal salts used are copper(II) acetate monohydrate (0.09 g), nickel(II) acetate tetrahydrate (0.11 g), zinc(II) acetate dihydrate (0.098 g), and cobalt(II) acetate tetrahydrate (0.11 g).

Biological Activity

Bacteria Culture

Antimicrobial activity was done at the Microbiology Laboratory of Physical Building, Kulliyah of Science, International Islamic University Malaysia. The bacteria were cultured following the previous report [19]. All strains, including *Escherichia coli* (ATCC 25922) and *Staphylococcus aureus* (ATCC 25923), were streaked on nutrient agar plates from stock stored at -80°C. 24 hours before the MIC assay, the strains were cultured on a nutrient medium at 37°C. Bacterial inocula were done by selecting 3 to 4 colonies from the agar plate and modifying the 0.5 Mc Farland standard solutions in nutrient broth. The turbidity of the bacteria was identified by measuring the optical density (OD) at 600 nm with a single-beam UV-Vis Spectrophotometer. The bacteria should exhibit an optimal OD of 0.1, 1.5 x 10^{-8} CFU/mL.

Antimicrobial Assay

The antibacterial assay was evaluated by minimal inhibitory concentration (MIC, µg/mL) [20]. MIC was determined through the two-fold serial broth microdilution technique in 96-well microtitration plates using a nutrient broth medium. The stock solutions of the synthesised compounds were prepared as 7000 µg/ml in dimethyl sulfoxide (DMSO) and diluted to a maximum of 5% solvent content with a sterile medium. 100 µL of Nutrient broth stock was added to each well, with the exception of the primary well. From that point forward, 200 µL of the stock compound was added into the first well of the plate, and serial dilutions were performed using a micropipette. Then, 100 µL of the new bacterium was added to all wells. After incubating at 37°C for 24 hours, the MIC value recorded is defined as the lowest concentration of the tested antimicrobial agents (expressed in µg/mL).

Computational Study

ADMET Analysis

The ADMET analysis of the synthesised compound was performed using SwissADME (http://www.swissadme.ch/) [21] and Pro-Tox II webpages (http://tox.charite.de/protox_II) [22]. The SMILES notations of the synthesised compounds obtained from ChemDraw were used as the input for ADMET evaluation.

Molecular Docking

The two-dimensional structures of synthesised compounds were sketched using ChemDraw to generate SMILES notation. Subsequently, the molecules were converted to 3D structures, optimised using the Auto Optimize tool in Avogadro 2.0 [23], and saved in the PDB format. For this study, both the mutant and wild type of *E. coli* DNA gyrase B were used as receptors. The crystallographic structures of both mutant and wild-type *E. coli* DNA gyrase B (PDB ID:1AJ6 and 4WUB) were downloaded from Protein Data Bank (http://www.pdb.org). 1AJ6 is a novobiocin-resistant mutant (R136H) of the N-terminal 24 kDa fragment of DNA gyrase B complexed with novobiocin at 2.3 angstroms resolution [24]. Meanwhile, 4WUB is an N-terminal 43 kDa fragment of the wild-type *E. coli* DNA gyrase B subunit grown under 100 mM KCl condition [25]. Initially, a control docking procedure was carried out by re-docking the co-crystallised ligands, novobiocin (1AJ6), and phosphoaminophosphonic acid-adenylate ester (4WUB) into the respective *E. coli* DNA gyrase B enzyme structures to parameterise the docking parameters.

Table 1. The grid centres and a number of points for proteins.

Grid box parameters	*Mutant 1AJ6*	*Wild-type 4WUB*
Grid centre x	60.767	13.625
Grid centre y	-7.795	20.657
Grid centre z	35.864	-12.237
No. of points x (Å)	50	50
No. of points y (Å)	50	50
No. of points z (Å)	50	50

Both proteins and molecules were prepared using AutoDockTools (ADT) version 1.5.6 (http://mgltools.scripps.edu). The bound ligand and crystal water molecules were removed from the target protein structure, followed by the addition of polar hydrogen atoms and Kollman partial charges before the protein structure was converted to the PDBQT format. For ligands, Gasteiger charges were assigned and saved in the PDBQT format. The docking was carried out using the AutoDock 4.2 package suite [26] by setting the appropriate size and centre of the grid box according to Table 1 while the grid spacing was set to 0.3750 Å. The docking was performed using the default-setting genetic algorithm as follows: i) the number of GA runs: 50; ii) population size : 150; iii) the number of energy evaluations : 2.5 million (with 2.0 Å clustered tolerance); and iv) the number of generations : 27000. As the active site of both proteins were known from previous literature, confirmation of active sites were determined by the blind docking. In blind docking, the grid box was set up to cover the whole protein. The results were viewed and analysed based on the interactions between the compound and protein using PyMOL [27].

RESULTS AND DISCUSSION

Synthesis and Physical Data

The ligand, *S*-benzyl-β-*N*-2-methoxybenzoyl dithiocarbazate (SB2OME), was the result of condensation reactions between SBDTC with 2-methoxybenzoyl chloride in the presence of potassium hydroxide as shown in Figure 1. SB2OME then reacted with the metal ions in ethanol with the general formula of $[M(SB2OME)_2]$, where M is Cu^{2+}, Zn^{2+}, $Co^{2+,}$ and Ni^{2+}. Table 2 displays the physical and analytical data for SBTDC, SB2OME, and its metal complexes. The obtained spectroscopic and analytical data supported all the suggested structures in the present report. Sharp melting points (over 1-3 °C) were observed for all compounds, indicating impurities-free. The overall yield for all compounds is generally around 60-75 %. All metal complexes have molar conductivities between 4.82-8.71 ohm^{-1} mol^{-1} cm^2, indicating they are not electrolytic. This finding is consistent with the fact that non-electrolyte conductivity values in DMSO solution are less than 50 ohm^{-1} mol^{-1} cm^2 [28].

Infrared Spectroscopy Spectra

Table 3 lists the selected vibration bands of the ligands and their metal complexes, along with their assignments. The spectrum of SB2OME showed sharp bands at 3209 cm^{-1} and 3121 cm^{-1}, which are attributed to υ(N–H) (Figure 2). These peaks are evidence that SBDTC's β-nitrogen is targeted by the 2-methoxybenzoyl group, which results in the formation of *S*-benzyl-β-*N*-2-methoxybenzoyl dithiocarbazate. The spectra of SB2OME show sharp and strong υ(C=O) at 1638 cm^{-1} in addition to the absorption bands comparable to those in SBDTC, demonstrating that a condensation reaction successfully produced the new substituted ligand. Due to strong υ(C=S) at 1048 cm^{-1} and 1046 cm^{-1}, respectively, both SBDTC and SB2OME showed their presence in the thione tautomeric form. In addition, the IR spectrum of SB2OME proves that it exists as a thione tautomer due to the absence of υ(S-H) at around 2603-2707 cm^{-1} and υ(O-H) peaks, which was consistent with the NMR results.

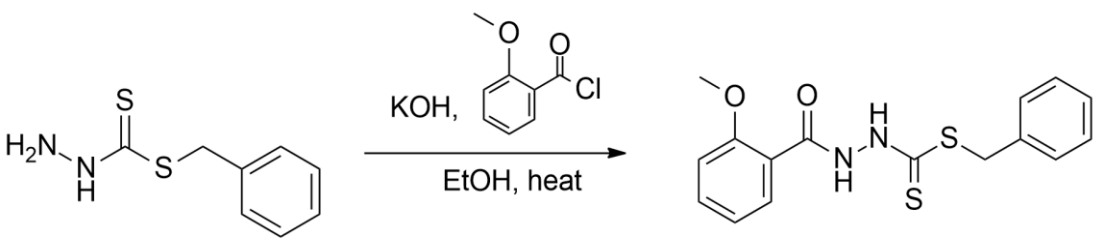

SBDTC SB2OME

Figure 1. Reaction scheme for the formation of SB2OME.

Table 2. Physical and analytical data of SB2OME and its complexes.

Compound	*Colour*	*M.p (ºC)*	*Yield (%)*	*Molar conductivity (ohm^{-1} mol^{-1} cm^2)*
SBDTC	White	122-123	60	-
SB2OME	White	156-158	65	-
$Cu(SB2OME)_2$	Black	230-232	63	4.82
$Zn(SB2OME)_2$	White	217-220	68	8.71
$Co(SB2OME)_2$	Green	260-263	62	7.89
$Ni(SB2OME)_2$	Brown	230-232	75	5.94

Tautomerism refers to the phenomenon where compounds such as SBDTC and other dithiocarbazate derivatives can rapidly interconvert by relocating a proton to become stable [29]. SB2OME can undergo thione-thiol-thionol-thiolol tautomerism, as shown in Figure 3, similar to the previous literature due to the presence of thiocarbonyl and carbonyl groups [18]. The thione-thiol tautomerism that occurred from the transition of a C=S double bond to a single C-S bond is due to the tautomerism of the dithiocarbazate ligand to its iminothiolate form [30]. Meanwhile, the conversion of a C=O double bond to a single bond of C-O occurs due to the tautomerism of the dithiocarbazate ligand to its enol form, resulting in thionol-thiolol tautomerism. It was found that all the SB2OME complexes showed a similar FTIR pattern (Figure 2), showing that all metal complexes would have similar interpretations on the vibration analysis, resulting in the same coordination mode with metal ions. As depicted in Figure 2, only one band corresponds to υ(N-H) around 3210 to 3179cm^{-1}. The disappearance of one peak, υ(N-H), from SBDTC, indicates that coordination occurred through the amino group. Plus, the shifting of υ(N-N) at 1327 cm^{-1} to lower frequencies in the metal complexes around 1294-1303 cm^{-1} shows evidence of metal coordination through the amino group. The metal complexes also depict a substantial negative shift in the υ(C=O) and υ(C=S), indicating the metal's coordination with carbonyl oxygen and thione sulphur, respectively [31]. As a result of losing one proton during complexation, SB2OME behaves as an uninegative tridentate *via* O, N, and S donors in the complexes (Figure 4).

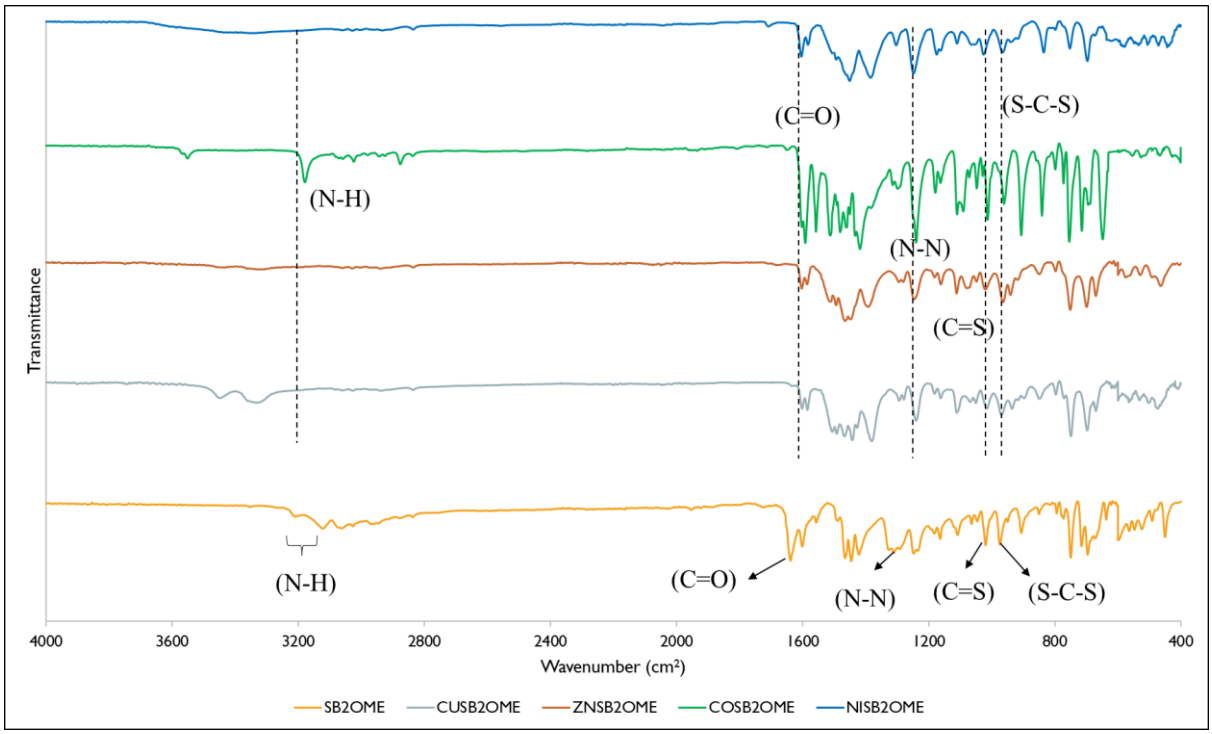

Figure 2. FTIR spectra of SB2OME and its complexes.

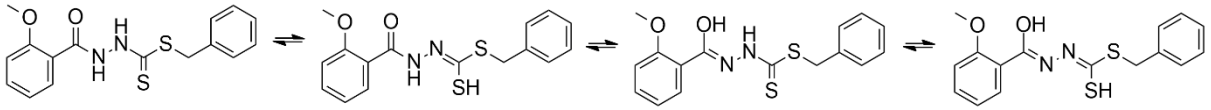

a – thione b – thiol c – thionol d - thiolol

Figure 3. Thione–thiol–thionol–thiolol tautomerism of SB2OME.

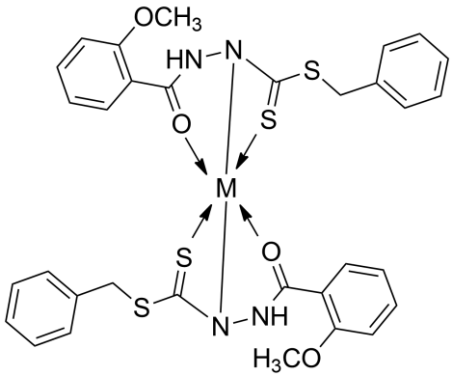

M = Cu, Zn, Co and Ni

Figure 4. Octahedral geometry of SB2OME's complexes.

Table 3. Selected IR bands of SBDTC, SB2OME and its metal complexes.

Compound	***IR bands (cm^{-1})***				
	υ(N–H)	υ(C=S)	υ(S-C-S)	υ(C=O)	υ(N–N)
SBDTC	3304, 3180	1048	952	-	1347
SB2OME	3209, 3121	1046	974	1638	1327
$Cu(SB2OME)_2$	3210	1019	971	1602	1294
$Zn(SB2OME)_2$	3206	1023	965	1604	1294
$Co(SB2OME)_2$	3179	1013	961	1602	1303
$Ni(SB2OME)_2$	3180	1020	963	1602	1294

Nuclear Magnetic Resonance Spectra

Table 4 presents the ^{1}H and ^{13}C NMR data of SB2OME. The chemical shift at δ_H = 11.5 and 10.5 ppm supports the attachment of the 2-methoxybenzoyl group to the β-nitrogen on SBDTC was caused by the two primary N-H groups. Due to its proximity to the electronegative nitrogen atom, this proton signal appeared to be deshielded. Additionally, resonance peaks associated with aromatic groups were found in the range of δ_H = 7.4-8.1 ppm. Besides, the methylene (-CH_2) proton between the sulphur atom and the aromatic ring could be clearly seen at δ_H = 4.5 ppm. At δ_H =3.8 ppm, a singlet peak representing the methyl proton of the methoxy group (O-CH_3) was detected. This methoxy group at the ortho position of the aromatic ring appeared at the most shielded area due to the shielding by the aromatic ring. From the ^{13}C NMR spectrum, the methylene (-CH_2) positioned between the S-C-S group and the aromatic ring was assigned at a chemical shift of 38.87 ppm. It was shielded due to electronegative sulfur residues near the CH_2 group. Meanwhile, the aromatic group has shielded the free CH_3 attached to electronegative oxygen, resulting in a signal at 56.23 ppm. In addition, resonances in the 165.16-112.58 ppm range are attributed to the carbon nuclei in the ligand's aromatic ring. Last but not least, due to the electronegative effect experienced by carbon atoms, both signals C=O and C=S were discovered in the least shielded area at 169.21 and 189.64 ppm, respectively. Furthermore, detecting both signals suggests that the Schiff bases primarily exist as the thione form in solution. However, if the thiol form were present, a signal at approximately 158 ppm would be observed [18]. Overall, the integration values from the ^{1}H-NMR and ^{13}C-NMR spectra closely matched the number of hydrogens and carbons suggested for SB2OME. The ^{1}H and ^{13}C NMR of all complexes were unable to be obtained due to their insolubility in deuterated solvents.

Table 4. ^{1}H-NMR and ^{13}C-NMR spectral data for SB2OME.

Compound	*^{1}H-NMR, δ (ppm)*				*^{13}C-NMR, δ (ppm)*				
	NH	S-CH_2	O-CH_3	Aromatic proton	C=S	C=O	O-CH_3	S-CH_2	Aromatic carbon
SB2OME	s, H (11.5), s, H (10.5)	s, 2H (4.5)	s, 3H (3.8)	m, (8.1-7.4 J = 7.5 Hz, 9H)	189.64	169.21	56.23	38.87	165.16-112.58

Table 5. Electronic spectra and magnetic moment data of SB2OME and its metal complexes.

Compound	*λ_{max}, nm (log e, cm^{-1} mol^{-1} L)*	*μ_{eff} (B.M.)*
SB2OME	286 (4.338), 259 (4.145)	-
$Cu(SB2OME)_2$	672 (2.662), 496 (3.072), 334 (4.24), 291 (4.366), 266 (4.26)	1.960
$Zn(SB2OME)_2$	322 (4.113), 300 (4.094), 259 (4.125)	diamagnetic
$Co(SB2OME)_2$	604 (2.17), 354 (4.04), 292 (4.235), 268 (4.303)	4.267
$Ni(SB2OME)_2$	718 (1.934), 351 (4.012), 288 (4.239), 265 (4.254)	3.288

Magnetic Moment and Electronic Spectral Data for Metal Complexes

Table 5 lists the metal complexes' electronic absorption spectral bands and magnetic moments. The magnetic moment of $Cu(SB2OME)_2$ was 1.960 B.M., suggesting one unpaired electron. As a result, an octahedral shape is anticipated to surround the copper(II) ion [32]. Due to the d^{10} electron configuration, $Zn(SB2OME)_2$ exhibits diamagnetic characteristics as reported by previous literature [33]. Thus, the predicted structure for the diamagnetic Zn(II) complex is octahedral with six coordinates. The cobalt(II) ion in $Co(SB2OME)_2$ was expected to be surrounded by an octahedral geometry based on the magnetic moment of the cobalt(II) complex (4.267 B.M) [34]. Last but not least, the magnetic moment value of paramagnetic $Ni(SB2OME)_2$ was 3.288 BM, confirming the presence of two unpaired electron configurations that point to an octahedral geometry [35]. Therefore, based on magnetic susceptibility studies, it was predicted that all of SB2OME's complexes would have an octahedral geometry, as illustrated in Figure 4.

From the electronic spectral data, high-intensity bands in the spectra of the SB2OME can be seen at 259 and 286 nm, which correspond to the benzene rings' $\pi \rightarrow \pi^*$ and $n \rightarrow \pi^*$ transitions, respectively [36]. Upon complexation, they exhibit a bathochromic shift at 288-300 nm compared to their free ligand. In addition, another band around 322-354 nm was assigned to the ligand-to-metal charge transfer (LMCT) transition [32]. Only the Zn(II) complex did not exhibit the low-intensity band at 500-800 nm, which is observed as a result of the forbidden $d \rightarrow d$ transition [9]. Copper(II) displays two low-energy $d \rightarrow d$ transitions at 496 and 672 nm, assigned to the $^{2}E_g \rightarrow {}^{2}T_{2g}$ transition, suggesting a distorted octahedral geometry. For distorted octahedral complexes, several weak bands are observed around $d \rightarrow d$ and often a broad tail in the near-infrared region due to the John-Teller effect [37]. Cobalt(II) and Nickel(II) complex showed a broad peak at 604 and 718 nm assigned to $^{4}T_{1g}(F) \rightarrow {}^{4}T_{2g}(F)$ and $^{3}A_{2g}(F) \rightarrow {}^{3}T_{2g}(F)$ transition, respectively, indicating an octahedral geometry of the complexes [38]. The electronic spectra further supported the proposed octahedral geometry from the magnetic moments study for all the complexes.

Antimicrobial Assay

The data provided in Table 6 presents the Minimum Inhibitory Concentration (MIC) values of various compounds against two common bacterial strains, *S. aureus* (ATCC 25923) and *E. coli* (ATCC 25922). MIC values represent the lowest concentration of an antimicrobial agent that inhibits the visible growth of a microorganism after overnight incubation. SB2OME exhibits a MIC value of 1750 µg/ml against *S. aureus* and *E. coli*. The presence of the benzyl group may account for the reduced activities of SB2OME compared to that of its precursor, SBDTC [18]. With MICs of 875 µg/ml, only $Cu(SB2OME)_2$ outperformed its free ligand as an inhibitor of *S. aureus*. However, all other complexes depicted bioactivities similar to SB2OME in *S. aureus*. Besides, with an inhibitory activity of 875 µg/ml, both $Cu(SB2OME)_2$ and $Co(SB2OME)_2$ are shown to be more active against *E. coli* than SB2OME. The modifications to the metal complexes make them compatible with the hydrophobic pocket at the bacteria's target site, boosting their capacity to bind to the microbe [39], [40]. This, in turn, improves the penetration and increases their bioactivity. Moreover, significant physicochemical changes occurring during chelation can be associated with the reported rise in metal complex efficiency against microorganisms.

For example, the introduction of metal altered the compounds' spatial geometry, increased their molecular weight, and added new redox characteristics. As a result, it promotes the delocalisation of π-electrons across the entire chelate ring. The delocalisation of π-electrons refers to the distribution of the electron density over a larger area within a molecule, especially when metal ions are introduced into the chelating compounds. As a result of this delocalisation, the electronic structure of the complex becomes more stabilised, eventually influencing various properties of the complex, such as its geometry, reactivity, and solubility. Thus, it makes the complexes more lipophilic in aqueous solutions, potentially increase the interactions with the biological membranes.

Upon comparison with common antibiotics, it becomes evident that SB2OME and its complexes exhibit higher MIC values against both *S. aureus* and *E. coli*. It indicates that the investigated compounds displayed a reduced efficacy when compared to the common antibiotics used in clinical practice. These compounds showed MIC values ranging from 875 µg/ml to 1750 µg/ml against both bacterial strains in comparison to gentamycin, novobiocin, ciprofloxacin, ampicillin, kanamycin, vancomycin and streptomycin, which typically have MIC values in a much lower range of 0.25 µg/ml to 64 µg/ml [41], these compounds demonstrate notably lower potency. Additionally, observations revealed significant variation in MIC values of the compounds between the two bacterial strains. *E. coli* is more selectively and significantly inhibited by most compounds than *S. aureus*. This finding differs from the past noteworthy discoveries in which gram-positive bacteria were often inhibited more severely than gram-negative bacteria. It has been found that the peptidoglycan of gram-negative bacteria is covered in an extra, very impermeable layer [42]. Teichoic acids, a particular class of polysaccharides present in the cell wall of gram-positive bacteria, are negatively charged and have aided the passage of positive metal ions [39].

It can be concluded that $Cu(SB2OME)_2$, $Zn(SB2OME)_2$, $Co(SB2OME)_2$, and $Ni(SB2OME)_2$ exhibited limited activity against both *S. aureus* and *E. coli*. The relatively higher MIC values suggested these compounds may not possess the requisite potency to be considered effective antimicrobial agents. Further investigations, including exploration of different concentrations, combination therapies, or modifications to the chemical structures of these compounds, may be warranted to enhance their antimicrobial activity and potential clinical relevance.

Table 6. Antimicrobial activity of SB2OME ligand and its metal complexes.

Compound	***MIC (ug/ml)***	
	S. aureus (ATCC 25923)	*E. coli* (ATCC 25922)
SBDTC	875	437
SB2OME	1750	1750
$Cu(SB2OME)_2$	875	875
$Zn(SB2OME)_2$	1750	1750
$Co(SB2OME)_2$	1750	875
$Ni(SB2OME)_2$	1750	1750
Gentamycin	32	16
*Gentamycin	6.25	4
*Novobiocin	0.25	64
*Ciprofloxacin	6.25	6.25
*Ampicillin	64	10
*Kanamycin	1.0	0.25
*Streptomycin	25	1.56
*Vancomycin	0.78	32

*Based on CLSI database.

Table 7. Physicochemical properties of investigated compounds.

Compounds	*MW (g/mol)*	*Log P*	*FC*	*HA*	*HD*	*MR*	*TPSA (Å²)*
SBDTC	198.31	1.66	0.12	1	2	57.11	95.44
SB2OME	332.44	2.78	0.12	2	2	93.41	107.75
$Cu(SB2OME)_2$	726.41	4.13	0.12	8	2	200.55	202.58
$Zn(SB2OME)_2$	728.24	4.13	0.12	8	2	200.55	202.58
$Co(SB2OME)_2$	721.8	4.13	0.12	8	2	200.55	202.58
$Ni(SB2OME)_2$	721.56	4.13	0.12	8	2	200.55	202.58

(MW-molecular weight, FC- Fraction Csp3, HA-Hydrogen bond acceptors, HD-Hydrogen bond donors, MR-Molar refractivity, TPSA- topological surface area)

Assessment of ADMET Properties

SwissADME evaluated the ADME properties of all the synthesised compounds by considering a few critical parameters for the potential antibacterial drug. To begin with, the physicochemical parameters predicted for the precursor, ligands, and metal complexes are presented in Table 7. SBDTC and the ligand SB2OME possess a molecular weight of less than 500, while the metal complexes have higher molecular weight due to the incorporation of the metal ions. Log P values for all compounds under investigation range from 1 to 5. According to Butina et al. (2002), lipophilicity substantially impacts the rate at which medicines are metabolised and eliminated from the body after adsorption [43]. In the case of medicines, efficient metabolism is important for regulating their concentration in the body and preventing toxicity. Lipophilicity can influence how rapidly a drug is metabolised because it affects its distribution within the body and its accessibility to metabolising enzymes. Therefore, the lipophilic characteristics of some compounds are essential in producing the antimicrobial effect. Besides, they all possess less than five hydrogen bond donor groups and less than 10 hydrogen bond acceptors, agreeing with Lipinski's rule of five. These properties are favourable for pharmacophore features to interact with residues within various biological targets [44]. However, all the metal complexes display a topological polar surface area of more than 140 $Å^{2,}$ [14] possibly due to their complex structure resulting from coordination.

Next, the predicted pharmacokinetic properties of all synthesised compounds were tabulated in Table 8. High GI absorption observed in the precursor and ligand suggests their high ability for gastrointestinal absorption, while all the metal complexes depicted low gastrointestinal absorption. Notably, none of them were predicted to penetrate the blood-brain barrier (BBB). SB2OME and its metal complexes, on the other hand, were observed to display expression for CYP3A4, indicating possible side effects. CYP3A4 is responsible for metabolising over 50% of the drugs commonly used in clinical and is predominantly found in the human liver [45]. Disabling CYP3A4 could potentially lead to drug toxicity by increasing exposure to other drugs administered concurrently [46]. Furthermore, all the compounds also possess low skin permeation, indicated by Log K_p value of -3.59 to -6.21 cm/s. The Log K_p, a coefficient derived from multiple linear regression, serves as an indicator of a molecule's permeability through the skin [47]. A lower Log K_p suggests decreased permeability. Substances with high skin permeability are more suitable for transdermal drugs than oral medications. Therefore, all compounds examined are more appropriate as oral drug candidates rather than constituents for transdermal drugs owing to their lower log Kp value. Overall, the result shows that the precursor and the ligand have a lower molecular weight below 500 g/mol, a lower topological surface area of 140 $Å^2$ and excellent GI absorption. Although the metal complexes have greater molecular weight and topological surface area due to their coordination [48-49] and poor GI absorption. However, they have more hydrogen bond acceptors than the precursor and ligand.

Table 8. Pharmacokinetics properties of investigated compounds.

Compounds	*GI absorption*	*BBB permeant*	*CYP3A4 inhibitor*	*Log K_p (skin permeation)*
SBDTC	High	No	No	-6.21
SB2OME	High	No	Yes	-5.69
$Cu(SB2OME)_2$	Low	No	Yes	-3.62
$Zn(SB2OME)_2$	Low	No	Yes	-3.64
$Co(SB2OME)_2$	Low	No	Yes	-3.6
$Ni(SB2OME)_2$	Low	No	Yes	-3.59

Table 9. Toxicity prediction of investigated compounds.

Compounds	*LD_{50} (mg/kg)*	*TC*	*CA*	*IM*	*MU*	*CY*
SBDTC	300	3	Active	Inactive	Active	Inactive
SB2OME	1500	4	Inactive	Inactive	Inactive	Inactive
$Cu(SB2OME)_2$	324	4	Inactive	Inactive	Inactive	Inactive
$Zn(SB2OME)_2$	324	4	Inactive	Inactive	Inactive	Inactive
$Co(SB2OME)_2$	324	4	Inactive	Inactive	Inactive	Inactive
$Ni(SB2OME)_2$	324	4	Inactive	Inactive	Inactive	Inactive

(TC-Toxicity class, CA-Carcinogenicity, IM-Immunotoxicity, MU-Mutagenicity, CY-Cytotoxicity)

Toxicity analysis of the compounds was also evaluated and reported in Table 9. SB2OME demonstrated an excellent toxicity profile according to a toxicity risk assessment, with an estimated LD_{50} of 1500 mg/kg, placing it in toxicity class 4. Cu(II), Zn(II), Co(II), and Ni(II) complexes all exhibited a similar toxicity class with an LD_{50} of 324 mg/kg. SBDTC, which has a category 3 with LD_{50} of 300 mg/kg, was the most toxic substance, as was to be predicted. Despite having equivalent or superior antibacterial activity, the LD_{50} values indicated that SB2OME and its complexes were safer or less toxic than its precursor, SBDTC. Furthermore, all compounds' toxicity analyses were conducted to ascertain their cytotoxicity, immunotoxicity, mutagenicity, and carcinogenicity. The findings showed that SBDTC was carcinogenic and active in mutagenicity, whereas SB2OME and its complexes were inactive in all the toxicity predictions. Therefore, according to the results of the toxicity studies, SBDTC alteration reduced the likelihood of toxicity, as evidenced by the SB2OME and its complexes.

Molecular Docking

One of the most common mechanisms of action of antibiotics is targeting DNA gyrase B, as reported by the class fluoroquinolone antibiotics. In conjunction with that, two target proteins of DNA gyrase B *E. coli* were chosen, which are from mutant and wild-type proteins with PDB IDs 1AJ6 and 4WUB, respectively. The choice of targeting mutant and wild-type DNA gyrase B of *E. coli* to discover the potential antibiotic leads is grounded by several key factors. DNA gyrase, an essential enzyme in bacteria, including *E. coli*, plays a crucial role in DNA replication and transcription by introducing negative supercoils into DNA. Inhibition of DNA gyrase can disrupt DNA replication and lead to bacterial cell death. Therefore, antibiotics targeting DNA gyrase often exhibit broad-spectrum activity against a wide range of bacterial pathogens beyond *E. coli*, and this potentially could lead to the development of antibiotics *that are* effective against other bacterial species as well. Mutations in DNA gyrase can confer resistance to antibiotics that target this enzyme, such as fluoroquinolones. Therefore, it is important to investigate both wild-type and mutant DNA gyrase B for the identification of compounds capable of overcoming existing resistance mechanisms [50-51].

The crystal structure of 1AJ6 was a mutant novobiocin R136H in which the arginine was substituted to histidine at amino acid 136. The two main differences between the structures of the mutant in 1AJ6 structure and the wild-type 1AJ6 involve a relatively strained conformation for His-136 and the presence of sequestered water in the volume vacated by the guanidinium group that arises from the replacement of the arginine [24]. The crystal structure of 4WUB, on the other hand, is a wild-type of *E. coli* DNA gyrase B subunit grown from 100 mM KCl condition [25]. Both crystal structures also have different co-crystallised ligands. The crystal structure of 1AJ6 was bound to novobiocin (NOV), whereas 4WUB was attached to phosphoaminophosphonic acid-adenylate ester (ANP). Both ligands are inhibitors that bind at the ATP binding site of DNA gyrase subunit B. It is observed that essential sites in the case of the mutant type are located in ASN46, GLU50, ASP73, ARG76, ILE78 and PRO79. Meanwhile, for the wild type of DNA gyrase, the important sites are located in ASN46, ASP73, ILE94, GLY102, LYS103, LEU115, HIS116, VAL118, GLY119 and VAL120. To explain the differences in active sites of DNA gyrase B between the mutant and wild-type enzymes of *E. coli*, these two proteins were aligned and inspected in PyMOL. NOV demonstrated a predilection for binding towards the outer region of the pocket site and vice versa with ANP, which is more susceptible inside the pocket site. Thus, both proteins were observed to have different binding subsites, as the inhibitors were coordinated in different directions, as shown in Figure 5.

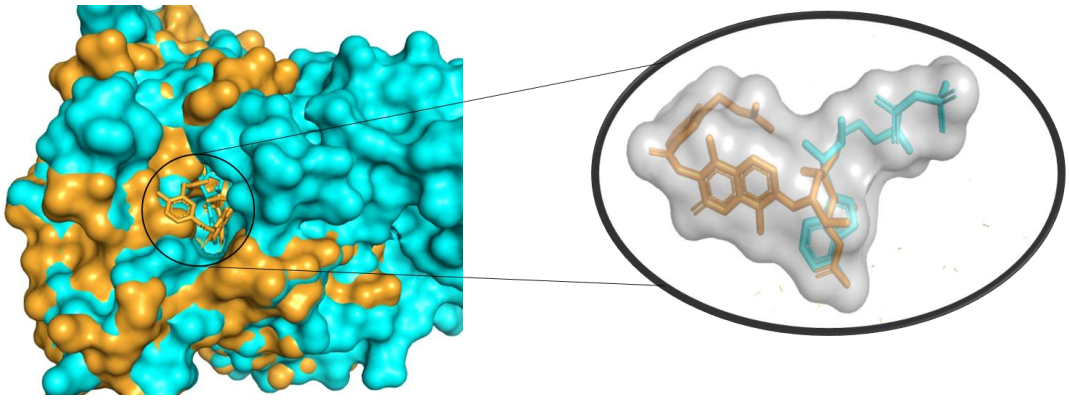

Figure 5. Alignment of NOV from mutant DNA gyrase B (orange) with ANP from wild-type DNA gyrase B (cyan) using PyMOL.

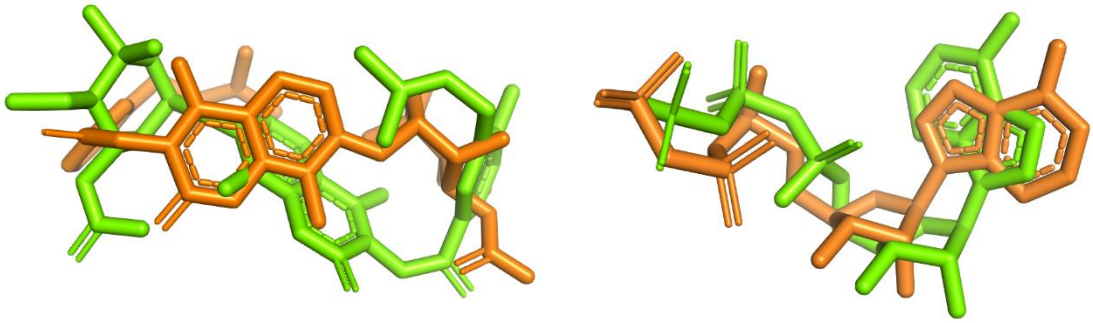

Figure 6. Redocking of NOV and ANP ligand into the gyrB *E. coli* potential active site. The ligand localisation in the 1AJ6 and 4WUB structures (orange) in comparison with the ligand localisation after redocking (green) using Pymol.

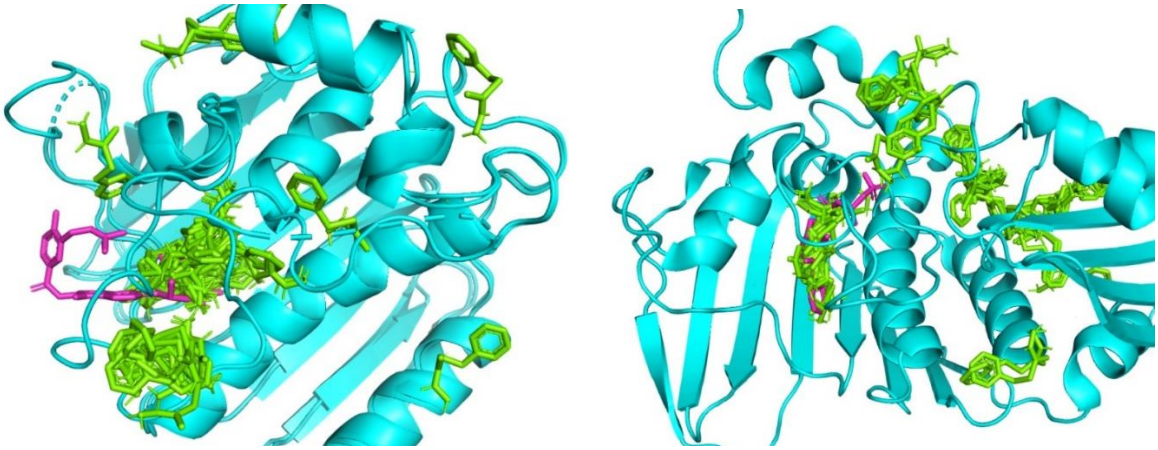

(a) (b)

Figure 7. Blind docking of SBDTC (green) with respective co-crytallised ligand (magenta) in (a) mutant DNA gyrase B and (b) wild-type DNA gyrase B.

Before docking was performed on all compounds, a redocking procedure was conducted to confirm the docking method effectively predicted the compounds' binding mode. The redocked NOV and ANP ligand-receptor complex produced binding energies of -7.23 and 12.33 kcal/mol, respectively. The RMSD values for the docked ligands in reference to their crystallised conformation were 1.796 Å and 1.047 Å, respectively. The alignment between the predicted and experimental positions is considered satisfactory when the RMS difference between the redocked and crystal ligand coordinates obtained is

less than 2 Å [52]. Therefore, the redocking outcomes demonstrated that the docking parameters were able to mimic the crystallised ligand conformation (Figure 6). Plus, the confirmation of active sites was further evaluated by blind docking. SBDTC was taken as an example compound, and results were shown in Figure 7. The fact that the blind docking, which explores the entire protein surface, identified a majority similar binding site to the local docking. This further supports that the local docking site was well-selected and likely represents a robust binding region on DNA gyrase.

The binding energy values in Table 10 show that all synthesised compounds exhibit stronger binding affinity towards the wild-type DNA gyrase compared to the mutant. All compounds display poorly binding with mutant DNA gyrase B conveyed those mutations imparted a significant change in the ability of compounds to bind to the protein. Plus, the ability to overcome AMR is also being reduced due to higher binding energy towards the mutant DNA gyrase B. Compound SB2OME had the highest binding affinity against 1AJ6 followed by $Zn(SB2OME)_2$, $Ni(SB2OME)_2$, SBDTC, $Cu(SB2OME)_2$ and $Co(SB2OME)_2$ with a binding energy of -6.71 kcal/mol, -6.50 kcal/mol, -6.42 kcal/mol, -6.18 kcal/mol, -5.53 kcal/mol and -5.45 kcal/mol respectively. The observed values reported the ligand shows stronger binding interactions than its respective metal complexes in mutant DNA gyrase B. A similar pattern was also observed in the wild-type DNA gyrase B, except for the cobalt complex. $Co(SB2OME)_2$ was observed to exert the highest binding affinity (-9.67 kcal/mol), followed by SB2OME, $Ni(SB2OME)_2$, $Zn(SB2OME)_2$, SBDTC and $Cu(SB2OME)_2$ with binding energies of -8.88 kcal/mol, -7.21 kcal/mol, -6.71 kcal/mol, -6.34 kcal/mol and -5.80 kcal/mol, respectively. The larger group of metal complexes was expected to create steric collisions and prevent correct intercalation with the proteins's active site, resulting in higher binding energies than SB2OME. Nevertheless, all investigated compounds were not comparable with the redocked control docking, NOV and ANP, which holds the lowest binding energies, -7.23 and -12.33 kcal/mol, respectively. Thus, in the sequence of highest to lowest binding affinity to the gyrB receptor, as stated,

a) R136 mutant DNA gyrase B - SB2OME > $Zn(SB2OME)_2$ > $Ni(SB2OME)_2$ > SBDTC > $Cu(SB2OME)_2$ > $Co(SB2OME)_2$

b) Wild type DNA gyrase B - $Co(SB2OME)_2$ > SB2OME > $Ni(SB2OME)_2$ > $Zn(SB2OME)_2$ > SBDTC > $Cu(SB2OME)_2$

Generally, the greater affinity of a compound is directly influenced by an increase in interactions, for example, hydrogen bonds, hydrophobic interactions and pi interaction. The strongest bonds between these interactions are hydrogen bonds. Hence, higher binding efficiency can be achieved when a ligand contains more hydrogen bonds. The co-crystallised NOV binds to the mutant DNA gyrase B with two hydrogen bonds, including ASN46 and ASP73. SB2OME, $Zn(SB2OME)_2$, $Ni(SB2OME)_2$, SBDTC and $Cu(SB2OME)_2$ also have at least three hydrogen bonds formed around the mutant DNA gyrase B with ASN46, GLU50, ASP73, GLY75, ARG76, GLY77 and THR165. However, the $Co(SB2OME)_2$-mutant DNA gyrase B complex exhibited only one hydrogen bond, explaining its lowest binding affinity. Aside from the hydrogen bond, the hydrophobic interaction was also discovered around the mutant protein. The co-crystallised NOV had six hydrophobic interactions with GLU50, ARG76, GLY77, ILE78, PRO79, and ILE94, which interact more than those found in the redocked NOV. The synthesised compounds were observed to favour hydrophobic interactions with the mutant DNA gyrase B rather than the hydrogen bond interaction, which is similar to their co-crystallised ligand, NOV. The collected data showed that the synthesised compounds form at least five hydrophobic interactions, including VAL43, ASP45, ASN46, ALA47, ASP49, GLU50, ALA53, VAL71, ARG76, PRO79, ALA90, ILE94, ALA100, THR165, VAL167.

Table 10. The binding energies of the control and synthesised compounds against the mutant and wild-type DNA gyrase.

Compounds	***Binding energy (kcal/mol)***	
	R136H mutant DNA gyrase B (PDB ID: 1AJ6)	**Wild-type DNA gyrase B (PDB ID: 4WUB)**
NOV/ANP	-7.23	-12. 33
SBDTC	-6.18	-6.34
SB2OME	-6.71	-8.88
$Cu(SB2OME)_2$	-5.53	-5.80
$Zn(SB2OME)_2$	-6.50	-6.71
$Co(SB2OME)_2$	-5.45	-9.67
$Ni(SB2OME)_2$	-6.42	-7.21

Table 11. AutoDock results show binding energy, interaction type, and amino acid residue against mutant DNA gyrase B (Important amino acids were bold).

Compounds	***Binding energy (kcal/mol)***	***Hydrogen bond***	***Hydrophobic interaction***
NOV (PDB ID: 1AJ6)	-	**ASN46, ASP73**	**GLU50, ARG76, GLY77, ILE78, PRO79, ILE94**
Redocked NOV	-7.23	**ASN46, ARG76,** GLY77, THR165	**GLU50, ILE78**, ILE94
SBDTC	-6.18	**ASP73**, GLY75, GLY77, THR165	VAL43, **ASN46**, ALA47, THR165, VAL167
SB2OME	-6.71	**ASP73, ARG76**, GLY77, THR165	VAL43, **ASN46**, ALA47, VAL71, THR165, VAL167
$Cu(SB2OME)_2$	-5.53	**ASN46, GLU50, ARG76**, GLY77	ASP49, **GLU50**, ALA53, ILE94, VAL120
$Zn(SB2OME)_2$	-6.50	**ASN46, GLU50, ARG76**	VAL43, **ASN46, ARG76, ILE78, PRO79,** ALA90, ILE94, THR165, VAL167
$Co(SB2OME)_2$	-5.45	**ASN46**	ASP45, **ASN46**, ASP49, **ARG76, PRO79**, ILE94, THR165
$Ni(SB2OME)_2$	-6.42	**ASN46, GLU50, ARG76**, GLY77, THR165	**ASN46, ILE78**, ALA90, ILE94, ALA100

On the other hand, against the wild-type DNA gyrase B, the redocked ANP exhibited the lowest binding energy of -12.33 kcal/mol with complete dominance from the hydrogen bond interaction (Table 12). The redocked ANP binds with the wild type of DNA gyrase B with fourteen amino acid residues, which include GLU42, ASN46, ASP73, GLY102, LYS103, TYR109, LEU115, HIS116, GLY117, VAL118, GLY119, VAL120, GLN335, LYS337, which twelve of them were similar with the co-crystallised ANP, justifying it highest binding affinity. Fewer hydrogen bonds were established between the synthesised compounds and the wild-type DNA gyrase. Instead, they preferred to form hydrophobic bond interaction with the wild-type DNA gyrase B protein except for SBDTC. $Co(SB2OME)_2$, which holds the highest binding affinities, is facilitated by three hydrogen bonds and eleven hydrophobic interactions. The three hydrogen bonds involving ASN46, ALA100, and GLY102, two of which were also found in co-crystallised ANP's binding. Meanwhile, the hydrophobic contacts were formed with ASN46, ILE78, PRO79, VAL93, ILE94, ALA100, LYS103, TYR109, VAL120, THR165, and VAL167 in which three of them were crucial amino acid residues. Most of the observed interaction with GLY102 contributed to the higher binding affinity as depicted by the cobalt complex and ANP. Plus, the absence of interaction with GLY102 in the SBDTC-wild type DNA gyrase B complex reduces its affinity. Thus, in Figure 8, all investigated compounds were concentrated at their respective binding subsites, suggesting they could act as a competitive inhibitor for the mutant and wild-type DNA gyrase B of *E. coli*.

Table 12. AutoDock results show binding energy, interaction type, and amino acid residue against Wild-type DNA gyrase B (Importance amino acids were bold).

Compounds	***Binding energy (kcal/mol)***	***Hydrogen bond***	***Hydrophobic interaction***
ANP (PDB ID: 4WUB)	-	**ASN46, ASP73**, **GLY102, LYS103**, TYR109, **LEU115, HIS116, VAL118, GLY119, VAL120**, GLN335, LYS337	GLU50, GLY77, ILE78, **ILE94**, ALA100, GLY101, GLY114, GLY117
Redocked ANP	-12.33	GLU42, **ASN46, ASP73**, **GLY102, LYS103**, TYR109, **LEU115, HIS116**, GLY117, **VAL118, GLY119, VAL120,** GLN335, LYS337	-

SBDTC	-6.37	ALA100, **VAL118, VAL120**, SER121	**LYS103**
SB2OME	-8.58	**GLY102, LYS103**	VAL43, **ASN46**, ALA47, ILE78, **ILE94, VAL120**, THR165, VAL167
$Cu(SB2OME)_2$	-6.26	**ASN46**, ALA100, **GLY102, LYS103**, GLY117	**ASN46**, ARG76, ILE78, PRO79, **ILE94**, TYR109, **VAL120**, THR165, VAL167
$Zn(SB2OME)_2$	-9.30	ALA100, **GLY102, LYS103**	**ASN46,** ARG76, ILE78, PRO79**, ILE94, LYS103**, TYR109, **VAL120**, THR165, VAL167
$Co(SB2OME)_2$	-9.60	ASN46, ALA100, **GLY102**	ASN46, ILE78, PRO79, VAL93, **ILE94**, ALA100, **LYS103**, TYR109, **VAL120**, THR165, VAL167
$Ni(SB2OME)_2$	-9.27	ALA100, **GLY102, LYS103**	ASN46, ARG76, ILE78, PRO79, **VAL120**, THR165, VAL167

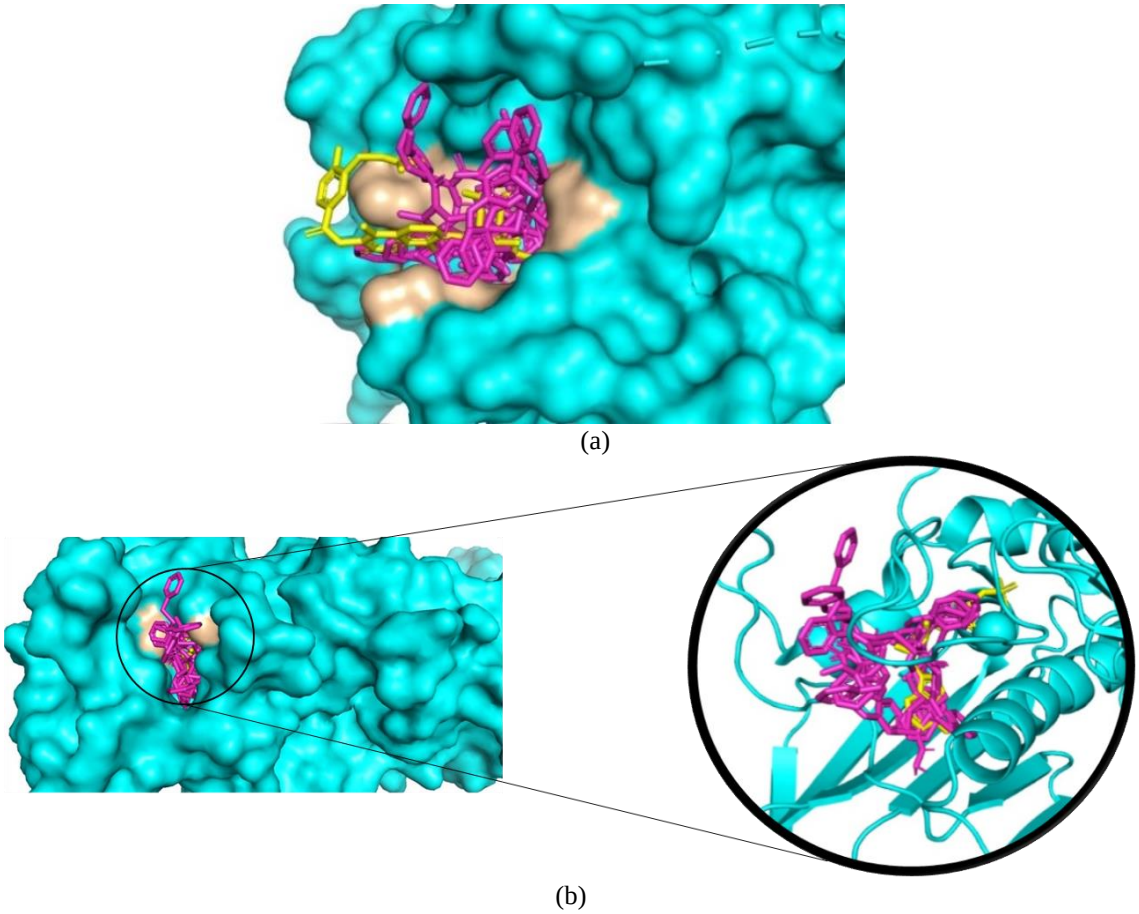

(a)

(b)

Figure 8. Localisation of all synthesised compounds (magenta) in reference with its control compounds (NOV/ANP) (yellow) in (a) mutant DNA gyrase B and (b) wild-type DNA gyrase B. The representations were visualised and rendered using PyMOL.

In the development of antimicrobial drugs, a drug candidate with the lowest binding energy in molecular docking is more likely to exhibit the lowest MIC value, indicating greater potency against bacteria. Consequently, it becomes crucial to compare *in-silico* and *in-vitro* results to evaluate whether these results match the proposed mechanisms of the targeted enzyme. If the obtained binding energies give a similar pattern corresponding to the MIC values, it suggests that the synthesised compounds operate through the proposed mechanism of action. On the other hand, any discrepancy in the patterns of the binding energies

and MIC values may indicate that the proposed mechanism is not the primary mode of action. The results presented in this study show that the MIC values of SB2OME and its metal complexes do not align with the binding energy patterns from either the mutant or the wild-type DNA gyrase B of *E. coli*. Therefore, according to this observation, it appears that SB2OME and its metal complexes do not inhibit the bacteria growth by targeting either mutant or wild-type DNA gyrase B in *E. coli*. However, it is important to acknowledge several limitations of molecular docking. Molecular docking primarily explores interactions between drug candidates and protein targets, such as nucleic acids or specific enzymes. In contrast, MIC assays offer a broader spectrum of interactions, considering the impact of antimicrobial agents on multiple cellular targets within bacteria, including cell wall synthesis, DNA replication, and protein synthesis [53]. Additionally, molecular docking often assumes protein structures to be rigid, whereas proteins are dynamic entities capable of undergoing structural changes upon ligand binding. Failing to account for such flexibility can lead to inaccurate predictions of ligand binding affinity and potency [54]. In contrast, MIC assays consider the entire bacterial cell, accounting for dynamic interactions between the drug and various components of the cell membrane and intracellular targets. Hence, these limitations highlight the need for additional computational methods, such as molecular dynamics simulations, to enhance the understanding of ligand binding and optimise drug efficacy against bacterial pathogens.

CONCLUSION

To conclude, this study focused on the synthesis and characterization of *S*-benzyl-*N*-2-methoxybenzoyl dithiocarbazate (SB2OME) and its complexes. The spectrochemical results show that SB2OME behaves as a tridentate ligand through the ONS donor atom, forming a neutral octahedral environment when coordinated with Cu(II), Zn(II), Co(II), and Ni(II) ions. The *in-vitro* antibacterial study showed that although SB2OME and its metal complexes show some degree of activity against *S. aureus* and *E. coli*, their efficacy, as indicated by MIC values, is notably lower when compared to the established antibiotics. The *in-silico* studies revealed moderate to good ADMET profiles for the investigated compounds. Additionally, the molecular docking results indicated that all the synthesised compounds exhibited greater compatible with wild-type DNA gyrase B of *E. coli* compared to the mutant one. Nevertheless, the difference between the binding energies and MIC assays suggests that DNA gyrase B may not represent the possible mechanism of action for the investigated compounds. As such, this work emphasises the need for structural modifications targeted at enhancing activity and effectiveness against harmful bacteria. Additionally, it advocates for exploring alternative computational methods to better elucidate the mechanism of action exerted by the newly synthesised compounds. Overall, the findings from this research are expected to assist in the development of antibacterial agents with improved efficacy.

ACKNOWLEDGEMENT

The authors thank the Department of Chemistry, Kulliyyah of Science, International Islamic University Malaysia Kuantan for providing laboratory facilities. An appreciation was also given to Associate Professor Dr. Nadiah Halim from the University of Malaya for her help in magnetic susceptibility analysis.

The authors declare that they have no conflict of interest.

REFERENCES

1. Zhou, N., Cheng, Z., Zhang, X., Lv, C., Guo, C., Liu, H., Dong, K., Zhang, Y., Liu, C., Chang, Y., Chen, S., Guo, X., Zhou, X. N., Li, M. and Zhu, Y. (2022) Global antimicrobial resistance: a system-wide comprehensive investigation using the Global One Health Index. *Infectious Diseases of Poverty*, **11(1)**, 1–16.

2. Murray, C. J., Ikuta, K. S., Sharara, F., Swetschinski, L., Robles Aguilar, G., Gray, A., Han, C., Bisignano, C., Rao, P., Wool, E., Johnson, S. C., Browne, A. J., Chipeta, M. G., Fell, F., Hackett, S., Haines-Woodhouse, G., Kashef Hamadani, B. H., Kumaran, E. A. P., McManigal, B. and Naghavi, M. (2022) Global burden of bacterial antimicrobial resistance in 2019: a systematic analysis. *The Lancet*, **399(10325)**, 629–655.

3. Evans, A. and Kavanagh, K. A. (2021) Evaluation of metal-based antimicrobial compounds for the treatment of bacterial pathogens. *Journal of Medical Microbiology*, **70(5)**.

4. Richard, H. H, Pierre, K. and Edward, I. S. (1996) Structural and Functional Aspects of Metal Sites in Biology. *Chemical Reviews*, **96(7)**, 2239–2314.

5. Domingos, S., André, V., Quaresma, S., Martins, I. C. B., Minas da Piedade, M. F. and Duarte, M. T. (2015) New forms of old drugs: improving without changing. *Journal of Pharmacy and Pharmacology*, **67(6)**, 830–846.

6. Gasser, G. (2015) Metal Complexes and Medicine: A Successful Combination. *Chimia*, **69(7–8)**, 442–446.

7. Renfrew, A. K. (2014) Transition metal complexes with bioactive ligands: mechanisms for selective ligand release and applications for drug delivery. *Metallomics*, **6**, 1324.

8. Sohtun, W. P., Kathiravan, A., Asha Jhonsi, M., Aashique, M., Bera, S. and Velusamy, M. (2022) Synthesis, crystal structure, BSA binding and antibacterial studies of Ni(II) complexes derived from dithiocarbazate based ligands. *Inorganica Chimica Acta*, **536**, 120888.

9. Bhat, R. A., Singh, K., Kumar, D., Kumar, A. and Mishra, P. (2022) Antimicrobial studies of the Zn(II) complex of *S*-benzyl-β-(*N*-2-methyl-3-phenylallylidene)dithiocarbazate. *Journal of Coordination Chemistry*, **75(7–8)**, 1050–1062.

10. Cavalcante, C. D. Q. O., Arcanjo, D. D. S., Silva, G. G. D., Oliveira, D. M. D. and Gatto, C. C. (2019) Solution and solid behavior of mono and binuclear Zinc(II) and Nickel(II) complexes with dithiocarbazates: X-ray analysis, mass spectrometry and cytotoxicity against cancer cell lines. *New Journal of Chemistry*, **43(28)**, 11209–11221.

11. Rosnizam, A. N., Hamali, M. A., Muhammad Low, A. L., Anouar, E. H., Youssef, H. M., Bahron, H. & Mohd Tajuddin, A. (2022) Palladium(II) complexes bearing N,O-bidentate Schiff base ligands: Experimental, in-silico, antibacterial, and catalytic properties. *Journal of Molecular Structure*, **1260**, 132821.

12. Kargar, H., Ashfaq, M., Fallah-Mehrjardi, M., Behjatmanesh-Ardakani, R., Munawar, K. S. and Tahir, M. N. (2022) Unsymmetrical Ni(II) Schiff base complex: Synthesis, spectral characterization, crystal structure analysis, Hirshfeld surface investigation, theoretical studies, and antibacterial activity. *Journal of Molecular Structure*, **1265**, 133381.

13. Payne, D. J., Gwynn, M. N., Holmes, D. J. and Pompliano, D. L. (2007). Drugs for bad bugs: Confronting the challenges of antibacterial discovery. *Nature Reviews Drug Discovery*, **6(1)**, 29–40.

14. Castillo-Morales, R. M., Carreño Otero, A. L., Mendez-Sanchez, S. C., da Silva, M. A. N., Stashenko, E. E. and Duque, J. E. (2019) Mitochondrial affectation, DNA damage and AChE inhibition induced by Salvia officinalis essential oil on Aedes aegypti larvae. *Comparative Biochemistry and Physiology Part C: Toxicology & Pharmacology*, **221**, 29–37.

15. Cavasotto, C. N., María, Aucar, G. and Adler, N. S. (2018) Computational chemistry in drug lead discovery and design. *Wiley Online Library*, **119(2)**.

16. Ferreira, L. G., Dos Santos, R. N., Oliva, G. and Andricopulo, A. D. (2015) molecules Molecular Docking and Structure-Based Drug Design Strategies. *Molecules*, **20**, 13384–13421.

17. Ali, M. A. and Bose, R. (1977) Metal complexes of schiff bases formed by condensation of 2-methoxybenzaldehyde and 2-hydroxybenzaldehyde with *S*-benzyldithiocarbazate. *Journal of Inorganic and Nuclear Chemistry*, **39**, 265–269.

18. How, F. N. F., Crouse, K. A., Tahir, M. I. M., Tarafder, M. T. H. and Cowley, A. R. (2008) Synthesis, characterization and biological studies of S-benzyl-β-*N*-(benzoyl) dithiocarbazate and its metal complexes. *Polyhedron*, **27(15)**, 3325–3329.

19. Malmberg, C., Yuen, P., Spaak, J., Cars, O., Tängdén, T. and Lagerbäck, P. (2016) A Novel Microfluidic Assay for Rapid Phenotypic Antibiotic Susceptibility Testing of Bacteria Detected in Clinical Blood Cultures. *Plos One*, **11(12)**, e0167356.

20. Gwaram, N. S., Ali, H. M., Khaledi, H., Abdulla, M. A., Hadi, H. A., Lin, T. K., Ching, C. L. and Ooi, C. L. (2012) Antibacterial evaluation of some schiff bases derived from 2-acetylpyridine and their metal complexes. *Molecules*, **17(5)**, 5952–5971.

21. Daina, A., Michielin, O. and Zoete, V. (2017) SwissADME: a free web tool to evaluate pharmacokinetics, drug-likeness and medicinal chemistry friendliness of small molecules. *Scientific Reports*, **7**.

22. Banerjee, P., Eckert, A. O., Schrey, A. K. and Preissner, R. (2018) ProTox-II: a webserver for the prediction of toxicity of chemicals. *Nucleic Acids Research*, **46**, W257.

23. Hanwell, M. D., Curtis, D. E., Lonie, D. C., Vandermeerschd, T., Zurek, E. and Hutchison, G. R. (2012) Avogadro: An advanced semantic chemical editor, visualization, and analysis platform. *Journal of Cheminformatics*, **4(8)**, 1–17.

24. Huey, R., Morris, G. M., Olson, A. J., Goodsell, D. S., Lindstrom, W., Sanner, M. F. and Belew, R. K. (1998) AutoDock4 and AutoDockTools4: Automated docking with selective receptor flexibility. *J. Comput. Chem.*, **19(2)**, 2785–2791.

25. Schrodinger, L. (2010) The PyMOL Molecular Graphics System, Version 1.3r1. *Scientific Research Publishing*.

26. Ali, I., Wani, W. A. and Saleem, K. (2013) Empirical formulae to molecular structures of metal complexes by molar conductance. *Synthesis and Reactivity in Inorganic, Metal-Organic and Nano-Metal Chemistry*, **43(9)**, 1162–1170.

27. Tarafder, M. T. H., Khoo, T. J., Crouse, K. A., Ali, A. M., Yamin, B. M. and Fun, H. K. (2002)

Coordination chemistry and bioactivity of some metal complexes containing two isomeric bidentate NS Schiff bases derived from S-benzyldithiocarbazate and the X-ray crystal structures of *S*-benzyl-β-*N*-(5-methyl-2-furylmethylene)dithiocarbazate and bis[*S*-benzyl-β-*N*-(2-furylmethylketone) dithiocarbazato]cadmium(II). *Polyhedron*, **21(27–28)**, 2691–2698.

28. Ravoof, T. B. S. A., Crouse, K. A., Tiekink, E. R. T., Tahir, M. I. M., Yusof, E. N. M. and Rosli, R. (2017) Synthesis, characterization and biological activities of S-2-or S-4-methylbenzyl-β-N-(di-2-pyridyl)methylenedithiocarbazate and Cu(II), Ni(II), Zn(II) and Cd(II) complexes.

29. Singh, M., Aggarwal, V., Singh, U. P. and Singh, N. K. (2009). Synthesis, characterization and spectroscopic studies of a new ligand [N′-(2-methoxybenzoyl)hydrazinecarbodithioate] ethyl ester and its Mn(II) and Cd(II) complexes: X-ray structural study of Mn(II) complex. *Polyhedron*, **28(1)**, 107–112.

30. Xuan Hung, N., Anh Quang, D., Thanh Tam Toan, T., -, al, Hamza Abbas, S., Mohammad Ali Murad, D., Hamza Abbas -, H., Mahmoud, W. A., M., Hassan, Z. and Russel W., Ali. (2020). Synthesis and spectral analysis of some metal complexes with mixed Schiff base ligands 1-[2-(2-hydroxybenzylideneamino)ethyl]pyrrolidine-2,5-dione (HL1) and (2-hydroxybenzalidine) glycine (HL2). *Journal of Physics: Conference Series*, **1660(1)**, 012027.

31. Abdalrazaq, E. A., Al-Ramadane, O. M. and Al-Numa, K. S. (2010). Synthesis and characterization of dinuclear metal complexes stabilized by tetradentate schiff base ligands. *American Journal of Applied Sciences*, **7(5)**, 628–633.

32. Emam, S. M., El-Saied, F. A., Abou El-Enein, S. A. and El-Shater, H. A. (2009) Cobalt(II), Nickel (II), Copper(II), Zinc(II) and Hafnium(IV) complexes of N′-(furan-3-ylmethylene)-2-(4-methoxyphenyl amino)acetohydrazide. *Spectrochimica Acta Part A: Molecular and Biomolecular Spectroscopy*, **72(2)**, 291–297.

33. Lever, A. B. P. (1984) Inorganic electronic spectroscopy. *Studies in Physical and Theoretical Chemistry*, **33**, 861–863.

34. Guo, L., Wu, S., Zeng, F. and Zhao, J. (2006) Synthesis and fluorescence property of terbium complex with novel schiff-base macromolecular ligand. *European Polymer Journal*, **42(7)**, 1670–1675.

35. Ramesh, P., AdilH, A., Mohammeda, N. -S., Siddappa, S., Muralidhar Reddy, P. and Pasha, C. (2016) Copper (II) Complexes of New Carboxyamide Ligands: Synthesis, Spectroscopic and Antibacterial Study. *International Journal of Advanced Research in Chemical Science (IJARCS)*, **3(8)**, 1–8.

36. El-Samanody, E. S. A., AbouEl-Enein, S. A. and Emara, E. M. (2018) Molecular modeling, spectral investigation and thermal studies of the new asymmetric Schiff base ligand; (E)-N'-(1-(4-((E)-2- hydroxybenzylideneamino) phenyl) ethylidene) morpholine-4-carbothiohydrazide and its metal complexes: Evaluation of their antibacterial and anti-molluscicidal activity. *Applied Organometallic Chemistry*, **32(4)**, e4262.

37. Ming, L. J. (2003). Structure and function of "metalloantibiotics. *Medicinal Research Reviews*, **23(6)**, 697–762.

38. Efthimiadou, E. K., Katsarou, M. E., Karaliota, A. and Psomas, G. (2008) Copper(II) complexes with sparfloxacin and nitrogen-donor heterocyclic ligands: Structure–activity relationship. *Journal of Inorganic Biochemistry*, **102(4)**, 910–920.

39. CLSI (2021) Performance standards for antimicrobial susceptibility testing, M100, 31st ed. *Clinical and Laboratory Standards Institute, Wayne, PA*.

40. Break, M. K. bin, Tahir, M. I. M., Crouse, K. A. and Khoo, T. J. (2013). Synthesis, characterization, and bioactivity of schiff bases and their Cd^{2+}, Zn^{2+}, Cu^{2+}, and Ni^{2+} complexes derived from chloroacetophenone isomers with *S*-benzyldithiocarbazate and the X-ray crystal structure of *S*-benzyl-β-*N*-(4-chlorophenyl) methylene dithiocarbazate. *Bioinorganic Chemistry and Applications*.

41. Butina, D., Segall, M. D. and Frankcombe, K. (2002) Predicting ADME properties in silico: methods and models. *Drug Discovery Today*, **7(11)**, S83–S88.

42. Oloruntoyin Ayipo, Y., Adesina Osunniran, W., Muhammad Badeggi, U., Olalekan Saheed, I., Adebayo Jimoh, A., Funmilayo Babamale, H. and Olawuyi Olaide, E. (2021) Synthesis, characterization and antibacterial study of Co(II) and Cu(II) complexes of mixed ligands of piperaquine and diclofenac, **8(2)**, 633–650.

43. Rendic, S. (1997) Human cytochrome P450 enzymes: a status report summarizing their reactions, substrates, inducers, and inhibitors. *Taylor & Francis S Rendic, FJD CarloDrug Metabolism Reviews*, **29(2),** 413–580.

44. Dresser, G. K., Spence, J. D. and Bailey, D. G. (2000) Pharmacokinetic-pharmacodynamic

consequences and clinical relevance of cytochrome P450 3A4 inhibition. *Clinical Pharmacokinetics*, **38(1),** 41–57.

45. Maciel Tabosa, M. A., Hoppel, M., Bunge, A. L., Guy, R. H. and Delgado-Charro, M. B. (2021) Predicting topical drug clearance from the skin. *Drug Delivery and Translational Research*, **11(2),** 729–740.

46. Okasha, R. M., Al Shaikh, N. E., Aljohani, F. S., Naqvi, A. and Ismail, E. H. (2019) Design of Novel Oligomeric Mixed Ligand Complexes: Preparation, Biological Applications and the First Example of Their Nanosized Scale. *International Journal of Molecular Sciences 2019*, **20(3)**, 743.

47. Syed Ali Fathima, S., Paulpandiyan, R. and Nagarajan, E. R. (2019). Expatiating biological excellence of aminoantipyrine derived novel metal complexes: Combined DNA interaction, antimicrobial, free radical scavenging studies and molecular docking simulations. *Journal of Molecular Structure*, **1178**, 179–191.

48. Saíz-Urra, L., Cabrera, M. A. and Froeyen, M. (2011) Exploring the conformational changes of the ATP binding site of gyrase B from Escherichia coli complexed with different established inhibitors by using molecular dynamics simulation: Protein-ligand interactions in the light of the alanine scanning and free energy decomposition methods. *Journal of Molecular Graphics and Modelling*, **29(5),** 726–739.

49. Roney, M., Issahaku, A. R., Forid, M. S., Huq, A. K. M. M., Soliman, M. E. S., Mohd Aluwi, M. F. F. and Tajuddin, S. N. (2023) In silico evaluation of usnic acid derivatives to discover potential antibacterial drugs against DNA gyrase B and DNA topoisomerase IV. *Journal of Biomolecular Structure and Dynamics*.

50. Holdgate, G. A., Tunnicliffe, A., Ward, W. H., Weston, S. A., Rosenbrock, G., Barth, P. T. and Timms, D. (1997) The entropic penalty of ordered water accounts for weaker binding of the antibiotic novobiocin to a resistant mutant of DNA gyrase: a thermodynamic and crystallographic study. *Biochemistry*, **36(32)**, 9663–9673.

51. Hearnshaw, S. J., Chung, T. H., Stevenson, C. E. M., Maxwell, A. and Lawson, D. M. (2015) The role of monovalent cations in the ATPase reaction of DNA gyrase. *Acta Crystallographica Section D: Biological Crystallography*, **71(4)**, 996–1005.

52. Bursal, E., Turkan, F., Buldurun, K., Turan, N., Aras, A., Çolak, N., Murahari, M. and Yergeri, M. C. (2021) Transition metal complexes of a multidentate Schiff base ligand containing pyridine: synthesis, characterization, enzyme inhibitions, antioxidant properties, and molecular docking studies. *BioMetals*, **34(2)**, 393–406.

53. Saikia, S. and Bordoloi, M. (2018) Molecular Docking: Challenges, Advances and its Use in Drug Discovery Perspective. *Current Drug Targets*, **20(5)**, 501–521.

54. Jakhar, R., Dangi, M., Khichi, A. and Chhillar, A. K. (2019) Relevance of Molecular Docking Studies in Drug Designing. *Current Bioinformatics*, **15(4)**, 270–278.